

Supplemental Appendix 1: Simple model of scan parameters and photobleaching

Calculations were implemented in Matlab and utilized the following parameters and assumptions:

The imaging volume considered consisted of: 300 x 300 x 50 voxels (x-y-z) (or 300 x 300 x 300 voxels for Supplemental Figure 1). We assume approximately 1 micron³ per voxel, and that the excitation volume for point-scanning methods is approximately 1 micron³.

Beginning with calculation of exposure time and line scan rates, we use:

V = volumes per second

t_{exp} = exposure time per voxel

R_S = galvanometer line scan rate (or z-scan rate for spinning disk)

Single point scanning:	$t_{exp,P} = 1/(V \cdot x \cdot y \cdot z)$	$R_{S,P} = V \cdot x \cdot z$
4-point scanning:	$t_{exp,P4} = 4/(V \cdot x \cdot y \cdot z)$	$R_{S,P4} = V \cdot x \cdot z/4$
Linear (Axial) scanning:	$t_{exp,LA} = 1/(V \cdot x \cdot y)$	$R_{S,LA} = V \cdot x$
Linear (Lateral) scanning:	$t_{exp,LL} = 1/(V \cdot x \cdot z)$	$R_{S,LL} = V \cdot z$
Spinning disk confocal (500 points):	$t_{exp,SDC} = 500/(V \cdot x \cdot y \cdot z)$	$R_{S,SDC} = V$
Oblique sheet (y-z') scanning:	$t_{exp,SA} = 1/(V \cdot x)$	$R_{S,SA} = V$
*Conventional light sheet (x-y):	$t_{exp,LISH} = 1/(V \cdot z)$	$R_{S,LISH} = V$
*Beam-scanned light sheet (x-y):	$t_{exp,BLISH} = 1/(V \cdot x \cdot z)$	$R_{S,BLISH} = V$

These variables (except *) are plotted as a function of volumetric imaging speed in Figure 3a and b (and Supplemental Figure 1a and b). Illumination power calculations considered the energy delivered to a voxel as equivalent to the number of fluorescent photons that would be produced. Reference energy E_{ref} was taken as the equivalent of confocal scanning a 300 x 300 area at 1 VPS using 0.5mW of illumination power:

$$E_{ref} = 0.11 \text{ nJ}$$

To produce equivalent fluorescence emission in each of the other configurations, we can then calculate the laser power needed to illuminate the sample to permit this amount of energy to reach each voxel. We ignore attenuation as a function of distance (assuming short pathlengths and minimal scattering). These powers P represent all of the light entering the sample. The second term, P' is calculated as the approximate power hitting a given voxel during a single volume scan (primary excitation only).

Single point scanning:	$P_P = E_{Ref}/t_{exp,P}$	$P'_P = E_{Ref}/t_{exp,P}$
4-point scanning:	$P_{P4} = 4E_{Ref}/t_{exp,P4}$	$P'_{P4} = E_{Ref}/t_{exp,P4}$
Linear (Axial) scanning:	$P_{LA} = E_{Ref}/t_{exp,LA}$	$P'_{LA} = E_{Ref}/t_{exp,LA}$
Linear (Lateral) scanning:	$P_{LL} = y \cdot E_{Ref}/t_{exp,LL}$	$P'_{LL} = E_{Ref}/t_{exp,LL}$
Spinning disk confocal (500 points):	$P_{SDC} = 500 \cdot E_{Ref}/t_{exp,SDC}$	$P'_{SDC} = E_{Ref}/t_{exp,SDC}$
Oblique sheet(y-z) scanning:	$P_{SA} = 2y \cdot E_{Ref}/t_{exp,SA}$	$P'_{SA} = 2E_{Ref}/t_{exp,SA}$
*Conventional light sheet (x-y):	$P_{LISH} = y \cdot E_{Ref}/t_{exp,LISH}$	$P'_{LISH} = E_{Ref}/t_{exp,LISH}$
*Beam-scanned light sheet (x-y):	$P_{BLISH} = E_{Ref}/t_{exp,BLISH}$	$P'_{BLISH} = E_{Ref}/t_{exp,BLISH}$

(factor of 2 in Oblique scanning denotes 50% emission side losses)

Values of P for each method (except *) are plotted as a function of volumetric imaging speed in Figure 3c.

From the per-pixel power values (P') we can estimate photobleaching effects based on Cranfill et al's [31] observation that fluorescent proteins following the trend of:

$$\log\left(\frac{t_1}{2}\right) = -\alpha \log(P') + c$$

where power is in μW but where $t_{1/2}$ corresponds to the half-life of the fluorophore scanned with a 512 x 512 field of view at 6 frames per second at power P' . Here, we used reference energy E_{ref} as the equivalent of confocal scanning a 512 x 512 area at 30 Hz using 0.5mW of illumination power (based on the capabilities of modern resonant confocals and [31]).

$$E_{ref} = 63 \text{ pJ}$$

Using $\alpha = 1.23$ and $c = 10.51$ (derived from Cranfill et al's reported values for EGFP $t_{1/2}$) we derive the fluorescence remaining after a given number of volumetric images as:

$$F(t_V) = F(t_{V-1}) \left(\frac{1}{2}\right)^{\frac{t_V}{t_{1/2}}}$$

Fluorescence decay curves were calculated for point, spinning disk confocal with 500 pints, axial line and oblique sheet techniques using exposure times and voxel-power (P') values listed above for the case of 10 VPS imaging as shown in Figure 3d (2 VPS results shown in Supplemental Figure 2c). However, these values account only for the photobleaching effect of the primary imaging beam, and not extraneous light illuminating the sample. The effects of this additional light were approximated assuming linear propagation of light without significant attenuation using the following conditions:

Single point scanning and spinning disk confocal:

A voxel at a given depth sees additional light for every z-plane acquired. Light exposure was estimated as $P'/\pi r^2$ where $r = zz \tan(40^\circ)$ for $zz = -z/2:z/2$. This partial power was used to estimate a corresponding $t_{1/2}$ with decays then accumulated over πr^2 exposures per z plane.

Linear (Axial) scanning (and beam-scanning light sheet):

A voxel sees the light surrounding the axial beam in the x-y plane. Effect assumed to be a cross approximately Gaussian spanning 5 pixels in x and y. Two sets of exposures per volumetric scan corresponding to the beam passing the voxel on 4 sides.

Oblique sheet (y-z') scanning (and conventional light sheet):

The light sheet is assumed to have a similar cross-section to the axial beam; a Gaussian across 5 pixels such that voxels adjacent to the sheet are partially exposed. One set of exposures are assumed per volumetric scan. Calculations include 2x required power to account for expected 50% emission-side losses.

Results of this analysis are shown in Figure 3e (10 VPS, $\alpha = 1.23$), Supplemental Figure 1d (300x300x300 voxel field of view), Supplemental Figure 2a (10 VPS, $\alpha = 1$), Supplemental Figure 2b (10 VPS, $\alpha = 1.23$), for conventional and beam-scanning light sheet), Supplemental Figure 2c (2 VPS, $\alpha = 1.23$).

Supplemental Appendix 2: Derivation of two-photon excitation v/s laser repetition rate

P_{peak} = peak power of pulse

T_p = pulse width

R_{rep} = laser repetition rate

E_p = energy per pulse

$$P_{peak} = \frac{P_{ave}}{T_p R_{rep}} = \frac{E_p}{T_p}$$

T_{int1} = integration time per pixel for point scanning:

$$T_{int1} = \frac{1}{N_x N_y N_z V}$$

where V is the volume rate, N_x , N_y and N_z are pixel numbers in the volume.

For imaging with multiple lateral (N_{dot}) points rather than 1, integration time per measurement (for the same volume rate) is

$$T_{intN} = T_{int1} N_{dot}$$

For oblique sheet scanning with the sheet extending along N_z integration time per measurement becomes

$$T_{intN} = T_{int1} N_{dot} N_z$$

When increasing the number of lateral points, the two-photon signal produced will be proportional to:

$$Sig_{2p} \propto T_{intN} R_{rep} \left(\frac{P_{peak}}{N_{dot}} \right)^2$$

Substituting

$$\begin{aligned} Sig_{2p} &\propto T_{intN} R_{rep} \left(\frac{P_{ave}}{T_p R_{rep} N_{dot}} \right)^2 \\ &= \frac{T_{intN}}{R_{rep}} \left(\frac{P_{ave}}{T_p N_{dot}} \right)^2 \\ &= \frac{T_{int1}}{N_{dot} R_{rep}} \left(\frac{P_{ave}}{T_p} \right)^2 \end{aligned}$$

For oblique sheet scanning then:

$$= \frac{N_z T_{int1}}{N_{dot} R_{rep}} \left(\frac{P_{ave}}{T_p} \right)^2$$

So laser repetition rate can be directly used to increase the number of points (locations) illuminated for the same signal detected if the same average power is maintained.

What does this do to the energy per point illuminated?

Energy per pulse incident on the tissue is:

$$E_p = \frac{P_{ave}}{R_{rep}}$$

Energy per point illuminated for N_{dot} points:

$$E_{p,pix} = \frac{P_{ave}}{N_{dot}R_{rep}}$$

So if repetition rate is decreased linearly as the number of points illuminated (laterally) increases, the energy seen per pulse, per pixel will remain the same.

Putting in numbers:

For a typical point-scanning Ti:Sapphire system:

$$P_{ave} = 100 \text{ mW}$$

$$R_{rep} = 80 \text{ MHz}$$

$$N_{dot} = 1$$

$$\text{Energy per pulse per pixel } E_{p,pix} = 1.25 \text{ nJ (below the 2nJ saturation limit)}$$

Assuming we are scanning a 400 x 400 x 100 volume at 5 volumes per second:

$$T_{int1} = 12.5 \text{ ns}$$

$$\text{Sig}_{2p} \propto 1.56 \times 10^8$$

For a lower repetition rate system with laterally distributed illumination:

$$P_{ave} = 100 \text{ mW}$$

$$R_{rep} = 200 \text{ kHz}$$

$$N_{dot} = 400$$

$$\text{Energy per pulse per pixel } E_{p,pix} = 1.25 \text{ nJ (below the 2nJ saturation limit) = same as for point scanning}$$

Assuming we are scanning a 400 x 400 x 100 volume at 5 volumes per second using laterally-distributed spots:

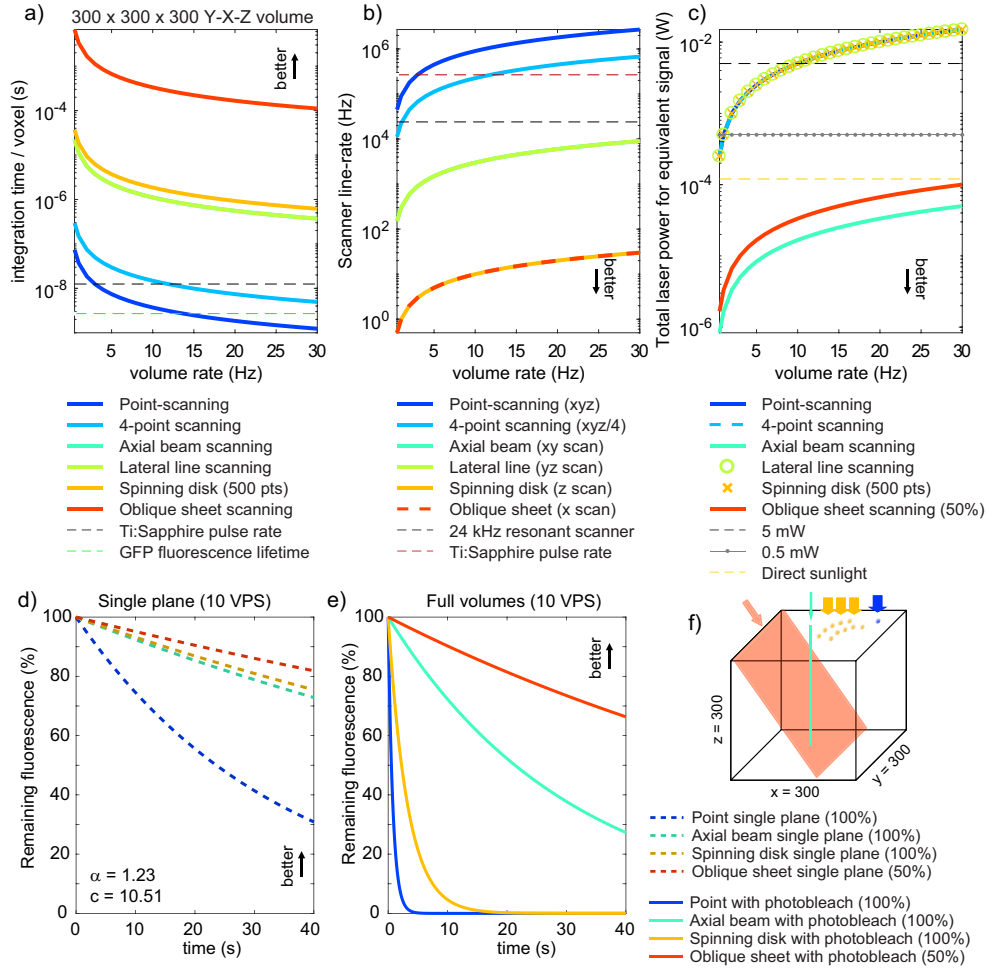
$$T_{int1} = 12.5 \text{ ns}$$

$$\text{Sig}_{2p} \propto 1.56 \times 10^8$$

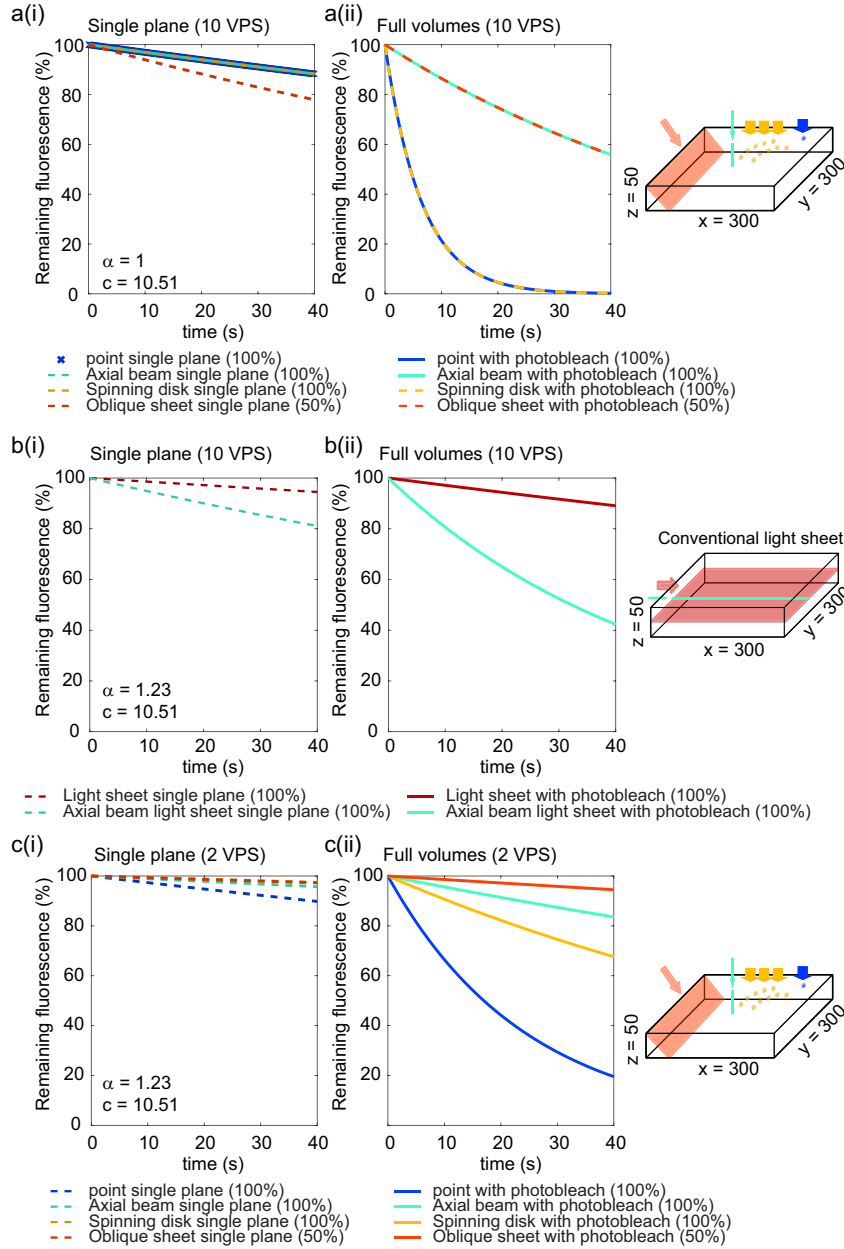
When using an oblique sheet, integration time can increase proportionally to the number of depths imaged simultaneously. So for 100 ($N_z = 100$) along an oblique sheet:

$$\text{Sig}_{2p} \propto 1.56 \times 10^{10}$$

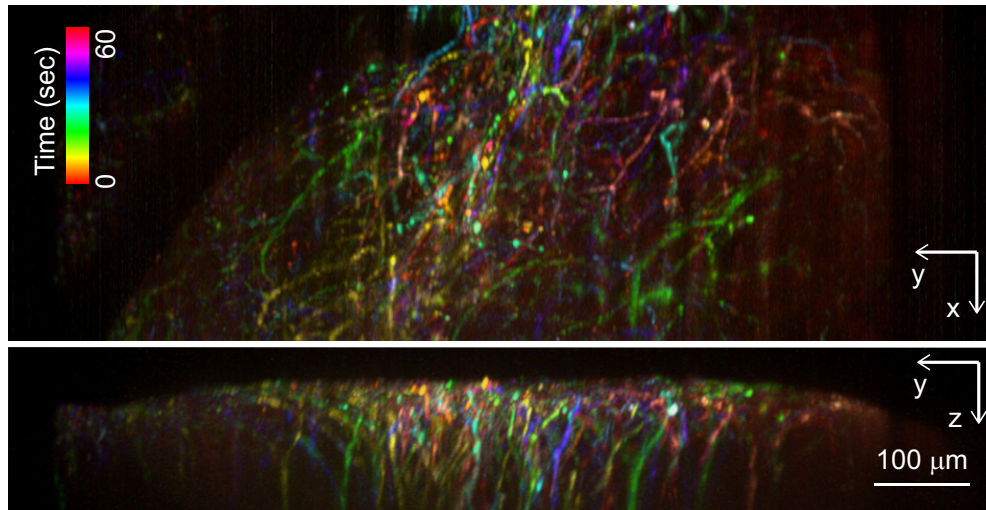
This factor of 100 or more helps to counteract 1) The faster volumetric imaging speeds desired compared to the 1 pulse per pixel limit of point-scanning 2) Reduced sensitivity for camera-based detection (although noise will be less problematic with longer integration times), 3) The approximation of minimal attenuation of the beam as it travels through the tissue and 4) Reduction in localization of focal spot for Gaussian sheet rather than high NA point (although this is likely also offset by group dispersion improvements).



Supplemental Figure 1. 300x300x300 voxel volume compared to Figure 3. Model-based comparisons between different volumetric imaging approaches in terms of a) per-voxel integration time, b) scanner line rate, c) total laser power needed for equivalent energy per voxel (based on 0.11 nJ energy deposited per pixel when point-scanning using 0.5mW at 1VPS) and d) predicted photobleaching dynamics for imaging at 10 VPS ignoring the effects of extraneous light during volumetric imaging and e) including photobleaching from extraneous light. See supplemental appendix for all model assumptions and parameters. f) All calculations based on a 300 x 300 x 300 xyz voxel volume. All results show that axially-extended line and sheet geometries deliver major benefits compared to point scanning – and effect that is even more striking when more depth layers are included.



Supplemental figure 2. Photobleaching models tests for different conditions. a(i) Primary ‘single plane’ photobleaching dynamics predicted for $\alpha = 1$, testing the case where photobleaching rates are linearly dependent on power. In this case, decays are the same for point-scanning, spinning disk confocal and axial beam scanning since all are calculated for the same power \times time = energy. The oblique sheet rate is faster because of the included 50% detection efficiency factor. a(ii) also uses $\alpha = 1$ but includes the effects of illumination of voxels by extraneous light during volumetric scanning. Here, even with linear photobleaching, point-scanning and spinning disk confocal exhibit much more severe photobleaching than axial beam and sheet imaging. b(i-ii) show photobleaching calculations for a conventional 90° light sheet geometry, demonstrating that supralinear photobleaching ($\alpha = 1.23$) implies that forming a light sheet from a brighter, scanning axial beam with a shorter effective integration time will cause more photobleaching than a lower irradiance light sheet with a longer effective integration time. c(i-ii) shows equivalent analysis to Figure 3d-e for 2 VPS scanning (a more achievable case for point-scanning confocal). Here, a lower but still significant rate of photobleaching is observed, with clear differences remaining between point-scanning v/s axial beam and sheet approaches.



Supplemental figure 3. SCAPE data acquired on the barrel cortex of an awake, behaving mouse capturing GCaMP6f dynamics in apical dendrites of layer 5 neurons. Images show maximum intensity projections from the top (x-y) and side (y-z), with color-coding representing the time at which pixels became active during a 60 second long recording. Figure 4b shows similar analysis on just a 6 second window of data, showing only around 6 distinct dendritic trees. Here, a large number of intertwined dendritic trees can be seen to have fired during the 60 second recording, demonstrating the power of SCAPE to capture real-time events throughout a large 3D field of view without requiring a-priori information. The dark diagonal stripe top left is a blood vessel. The active region corresponds to the area above the location of 100nL of AAV9.Syn.GCaMP6f into layer 5.